SUPPORTING INFORMATION

Mesoporous Co-B-N-H nanowires: a superior catalyst for hydrous hydrazine decomposition to generate hydrogen

FanYang[a,b], Yuan Zhi Li[a,c], Wei Chu[d*], Chun Li[a,b] and D.G. Tong[a,b*]

[a]*Mineral Resources Chemistry Key Laboratory of Sichuan Higher Education Institutions, College of Materials and Chemistry & Chemical Engineering, Chengdu University of Technology, Chengdu 610059, China. E-mail: tongdongge@163.com; Fax: +86-28-8407 9074*

[b]State Key Laboratory of Oil and Gas Reservoir Geology and Exploitation, Chengdu University of Technology, Chengdu 610059, China.

[c]Institute of Coal Chemistry, Chinese Academy of Science, Taiyuan 030001, China

[d]*College of Chemical Engineering, Sichuan University, Chengdu 610065, China. E-mail: chuwei1965@foxmail.com; Fax: +86-28-8540 3397*

Summary: 22 Pages; 1 Table; 31 Figures;

Table S1 Catalytic performance of different catalysts for N_2H_4 decomposition

Samples	Temperature/ ºC	S_{Co}/m^2 g^{-1}	H_2 generation volume/mL	H_2 selectivity /%	Time/min	TOF /min^{-1}	TTON	ATOF/ min^{-1}
$CoB_{0.358}N_{0.286}H_{0.251}$ nanowires in this work	293K	72.8	2240.0	100.0	17	76.0	133020	73.9
Conventional Co-B in this work	293K	18.7	22.8	1.02	91	4.83	-	-
Conventional Co-B after SPP treatment with NH_4Cl	293K	18.8	149.6	6.67	60	20.9		
Co-B nanowires in our work	293K	55.0	545.1	24.3	24	15.1	-	-
$CoB_{0.336}N_{0.215}H_{0.143}$ obtained in our work after SPP for 2 min	293K	48.6	1486.4	66.4	33	40.5	-	-
$CoB_{0.292}N_{0.113}H_{0.072}$ obtained in our work after SPP for 1 min	293K	45.8	1151.3	51.4	49	25.1	-	-
Co-B obtained in our work after SPP for 0.5 min	293K	16.2	17.9	0.799	82	4.68	-	-
In situ Rh_4Ni[16]	298K	-	89.6	100.0	160	0.25	-	-
In situ $Ni_{0.93}Pt_{0.07}$[17]	298K	-	89.6	100.0	190	0.0021	-	-
In situ $Ni_{0.95}Ir_{0.05}$[18]	298K	-	89.6	100.0	390	0.26	-	-
NiFe[19]	298K	-	89.6	100.0	190	-	-	-
In situ $Rh_{4.69}Ni$/graphene[20]	298K		89.6	100.0	49	1.91	-	-
Ni-Al_2O_3-HT[21]	303K	-	-	93.0	70	0.033	-	-
$NiPt_{0.057}/Al_2O_3$[22]	303K	-	70.2	98.0	11.5	0.28	-	-
$NiIr_{0.059}/Al_2O_3$[23]	303K	-	-	99.0	12.5	0.21	-	-
Monodispersed Ni_3Fe nanospheres / C[24]	293K	-	224.0	100.0	27	9.26	15840	8.8
9.86wt%Fe-B/MWCNTs[27]	298K	78.7	4345.6	97.0	15.2	67.2	114480	63.6
NiMoB-$La(OH)_3$[28]	323K	-	136.0	100.0	15	0.24	-	-
Amorphous $Ni_{0.9}Pt_{0.1}/Ce_2O_3$[29]	298K	-	172.0	100.0	43	0.47		
Co-B honeycomb[40]	298K	90.2	1872.6	41.8	13	12.6	18360	10.2
Co-B nanospheres[43]	298K	81.1	954.2	21.3	23	5.34	-	-

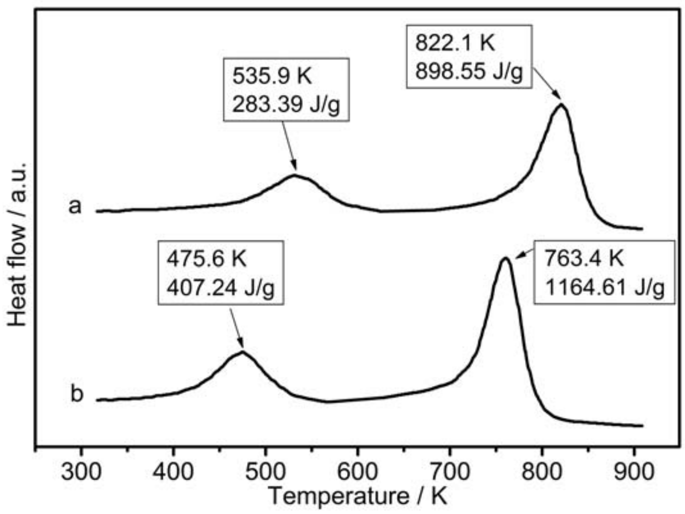

Fig.S1 DSC profiles of (a) Co–B–N–H nanowires and (b) Conventional Co-B amorphous alloy.

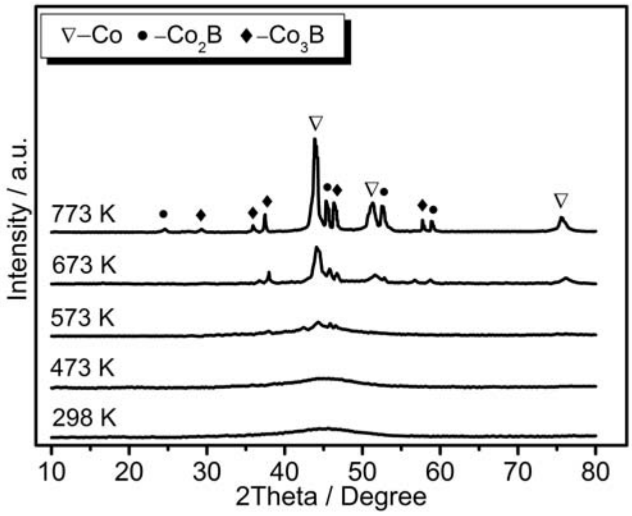

Fig.S2 XRD patterns of the conventional Co-B amorphous alloy treated at different temperatures.

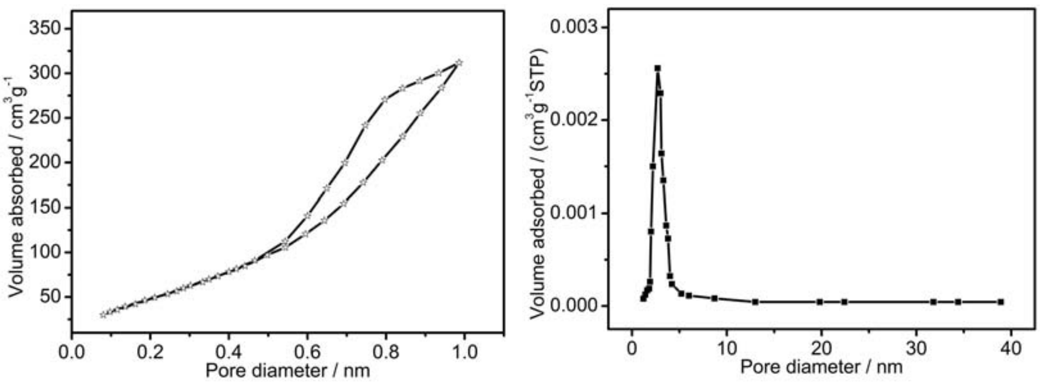

(a) (b)

Fig.S3 (a) Nitrogen sorption isotherms and (b) the corresponding pores diameter distribution of the as-prepared Co–B–N–H nanowires.

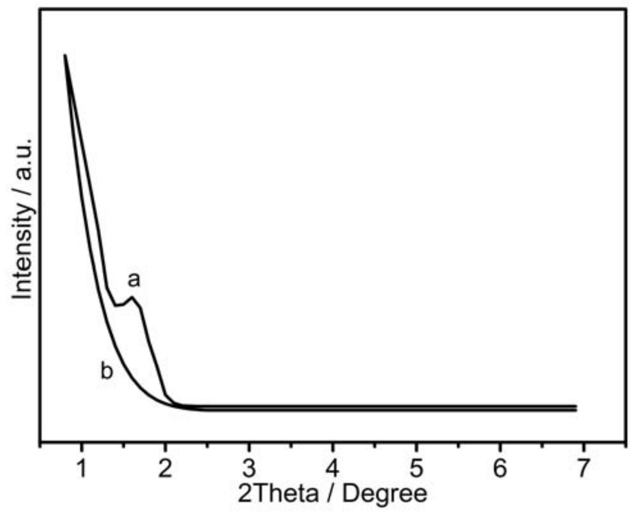

Fig.S4 Small angle XRD patterns of (a) Co–B–N–H nanowires and (b) Conventional Co-B amorphous alloy

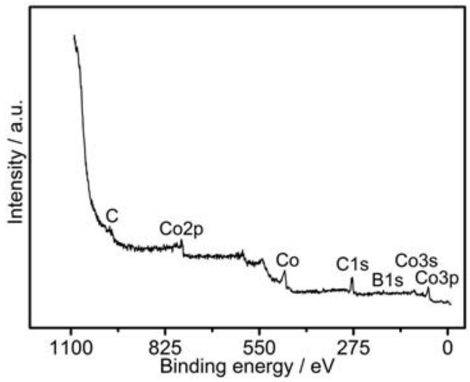

(a)

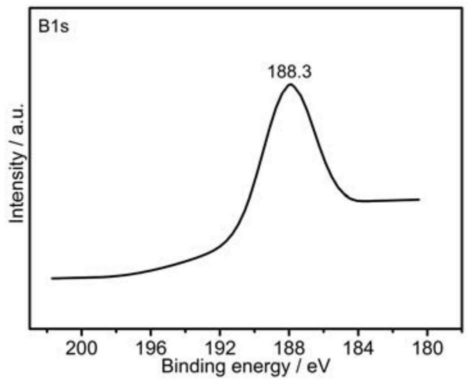

(b)

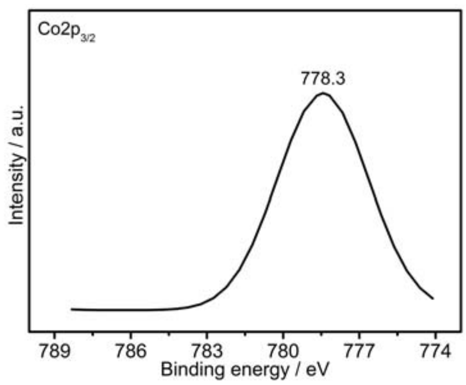

(c)

Fig.S5 XPS spectra for the conventional Co–B amorphous alloy: (a) survey spectrum, (b) B1s and (c) $Co2p_{3/2}$ spectra.

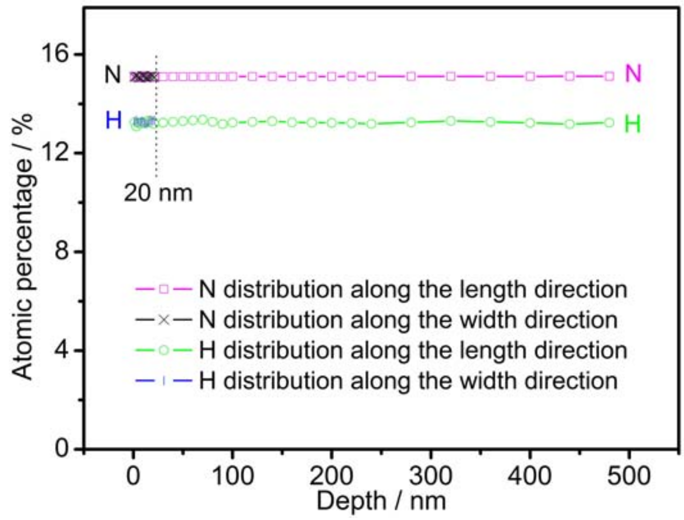

Fig.S6. The depth distribution of N and H along the width direction (0-20nm) and length direction (0-480nm) of Co-B-N-H nanowires obtained from the ToF-SIMS depth profiles.

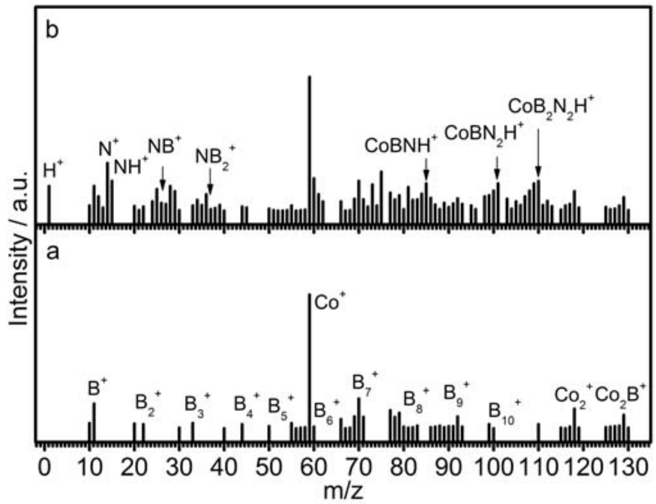

Fig.S7 ToF-SIMS spectra of (a) the conventional Co–B amorphous alloy and (b) the conventional Co–B after treated by SPP with NH_4Cl.

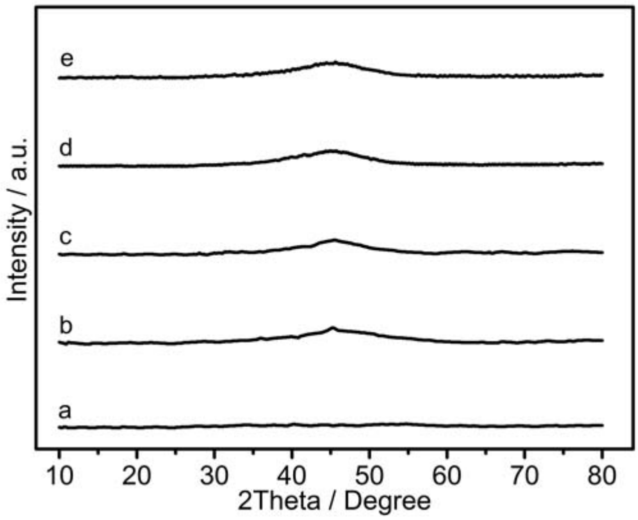

Fig.S8 XRD patterns of the Co–B–N–H nanowires prepared during SPP: (a) 0.5 min; (b) 1 min; (c) 2 min; (d) 5 min; (e) 10 min.

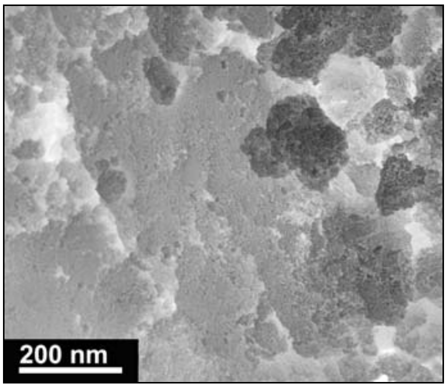

(a)

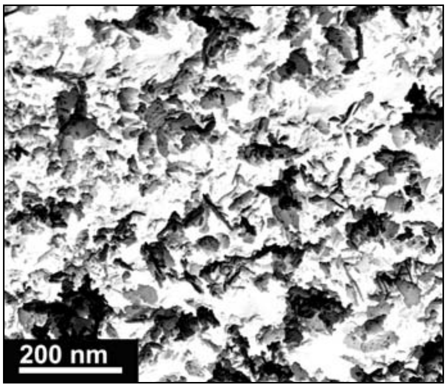

(b)

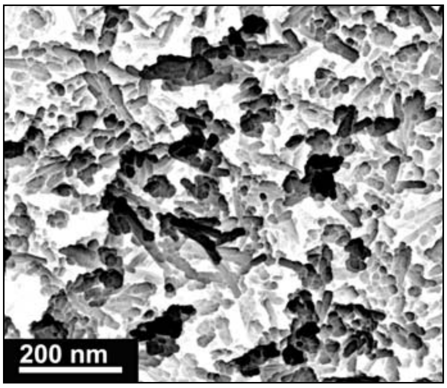

(c)

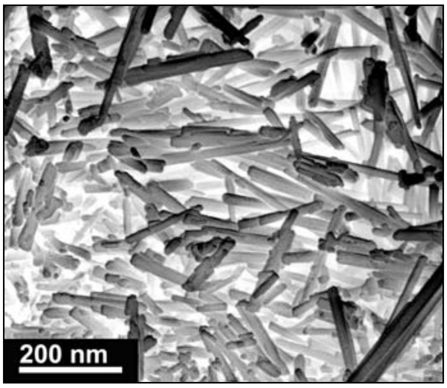

(d)

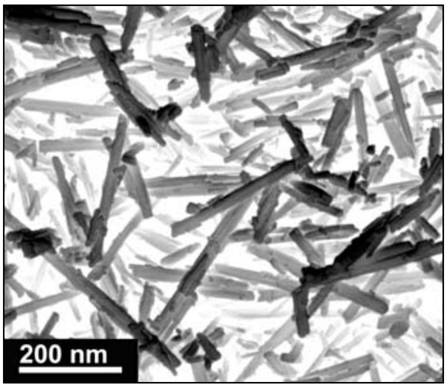

(e)

Fig.S9 STEM images of the Co–B–N–H nanowires prepared during SPP: (a) 0.5 min; (b) 1 min; (c) 2 min; (d) 5 min; (e) 10 min.

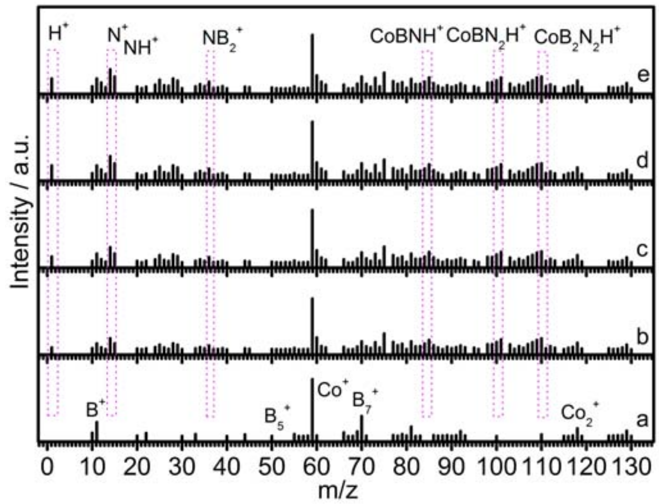

Fig.S10 ToF-SIMS spectra of the Co–B–N–H nanowires prepared during SPP: (a) 0.5 min; (b) 1 min; (c) 2 min; (d) 5 min; (e) 10 min.

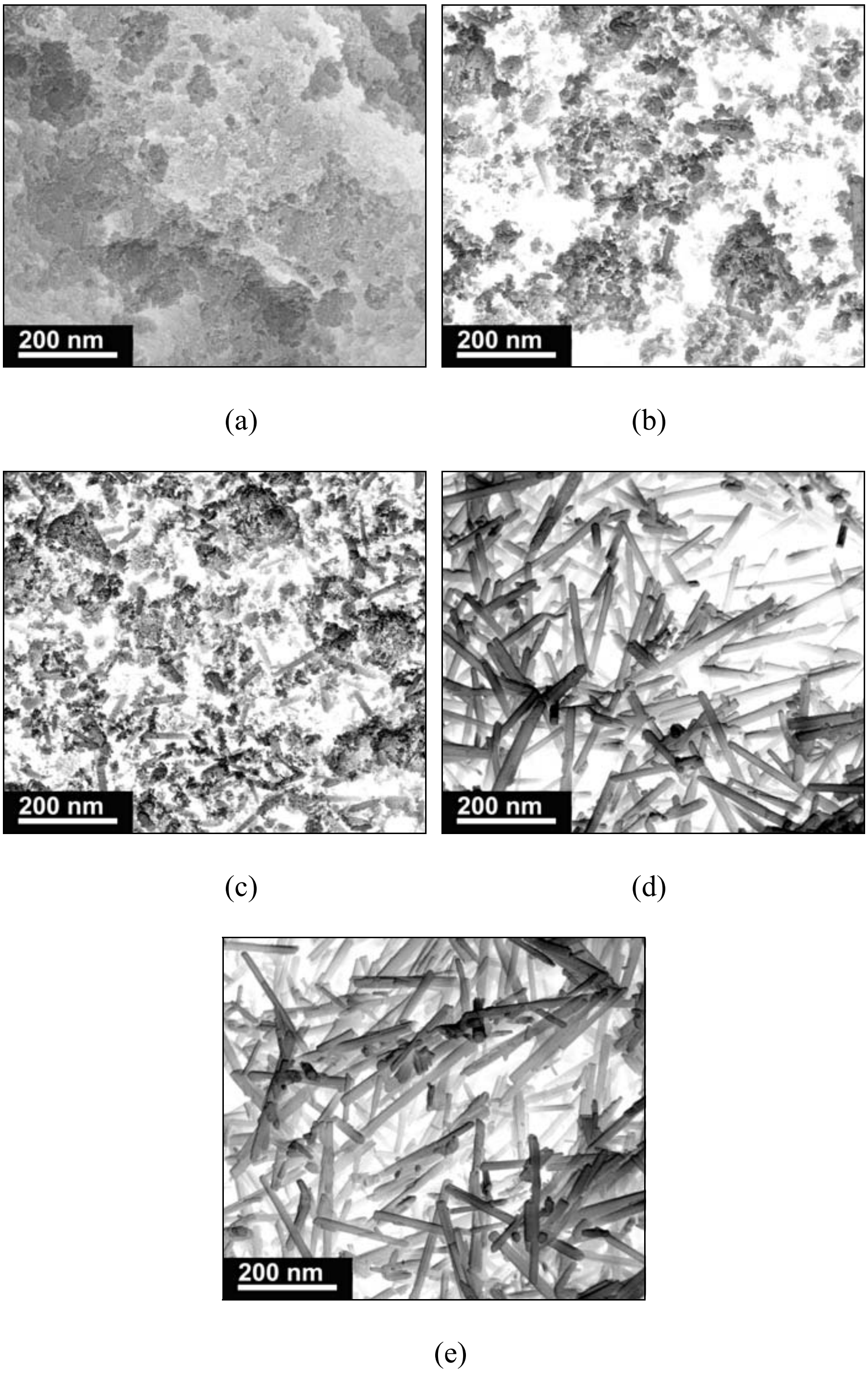

Fig.S11 STEM images of the Co–B–N–H nanowires obtained with different concentration of Brij-58: (a) 0 M, (b) 0.01 M, (c) 0.02M, (d) 0.05 M, (e) 0.1 M.

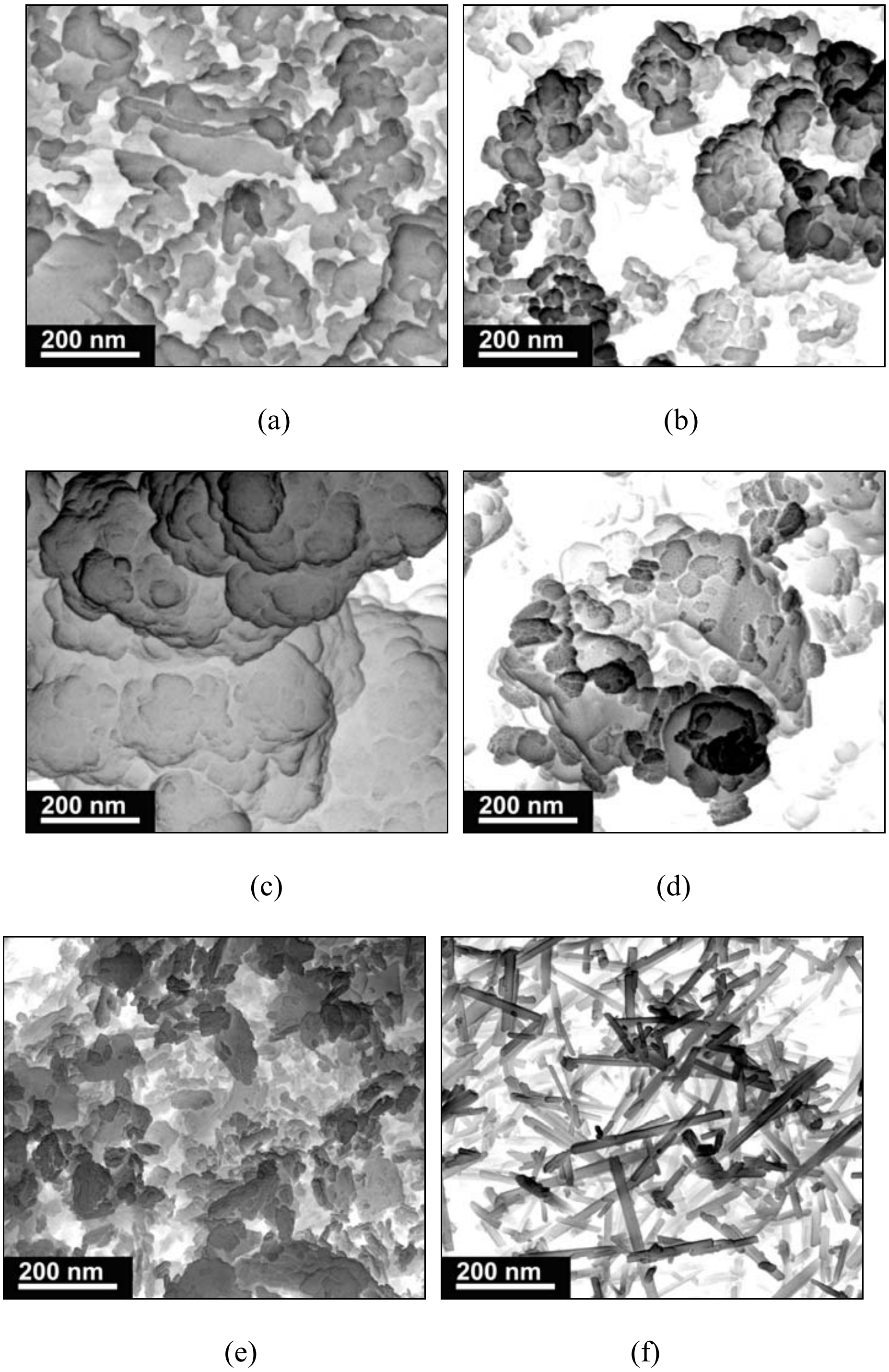

Fig.S12 STEM images of the Co–B–N–H nanowires prepared by SPP with (a) PVA; (b) PVP; (c) P123; (d) ethylenediamine; (e) SDBS and (f) either of (a)–(e) after additional of Brij-58.

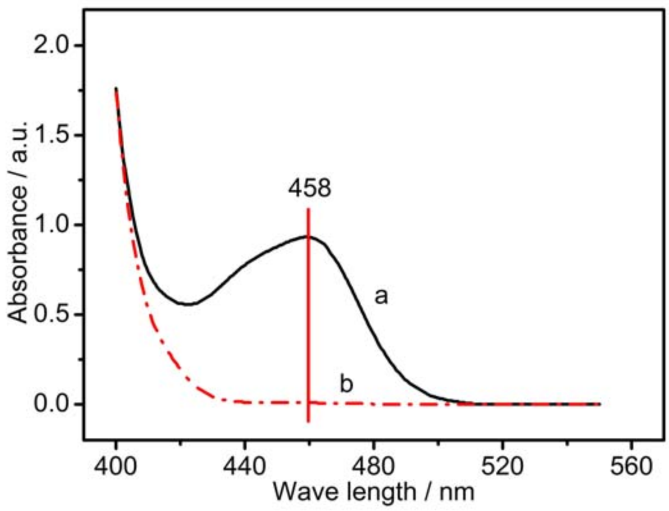

Fig.S13 Typical UV-Vis spectra of hydrous hydrazine (a) before and (b) after the completion of hydrazine decomposition reaction over Co–B–N–H nanowires.

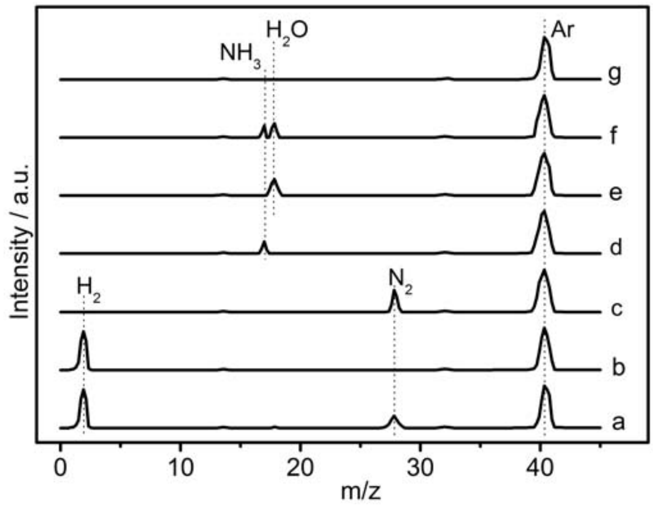

Fig.S14 Mass spectral (MS) profile of (a) the gases released from the complete decomposition of hydrous hydrazine at room temperature over Co–B–N–H nanowires; (b) H_2; (c)N_2; (d) NH_3; (e) H_2O; (f) NH_3+H_2O; and (g) carrier Ar.

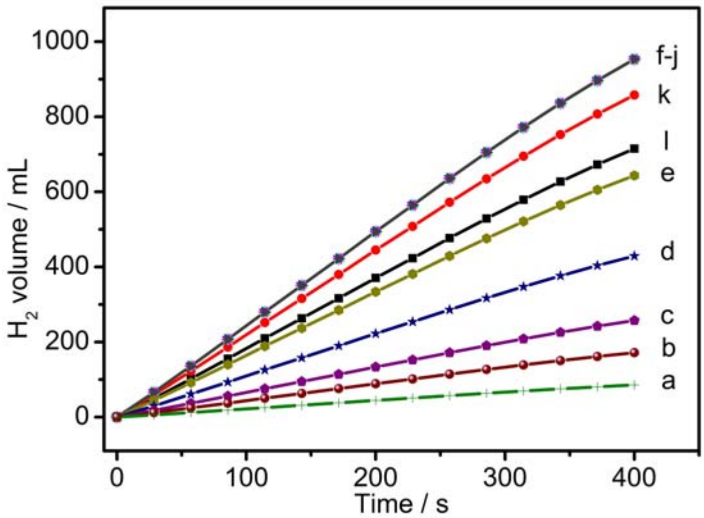

Fig.S15 Hydrogen released from 20mL N_2H_4 solution with different concentrations (a) 0.01, (b) 0.02, (c) 0.03, (d) 0.05, (e) 0.075, (f) 0.1, (g) 0.2, (h) 0.5, (i) 1, (j) 5, (k) 7.5 and (l) 10.0molL^{-1}in the presence of 4.6mg Co–B–N–H nanowires.

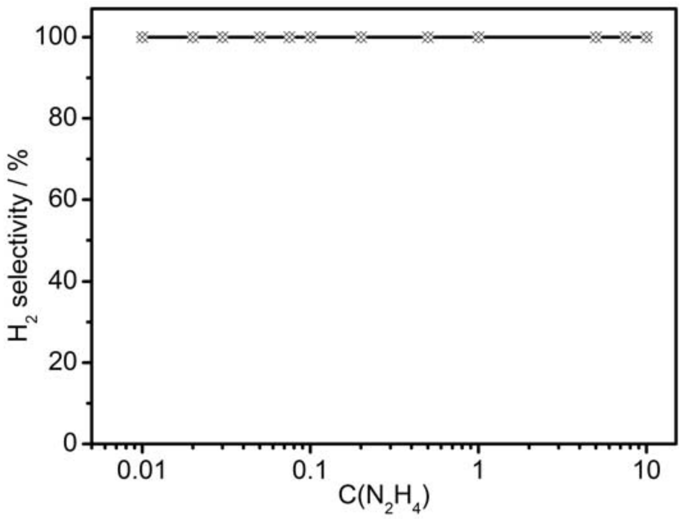

Fig.S16 Hydrogen selectivity versus N_2H_4 concentrations for the decomposition of N_2H_4 over 4.6mg Co–B–N–H nanowires.

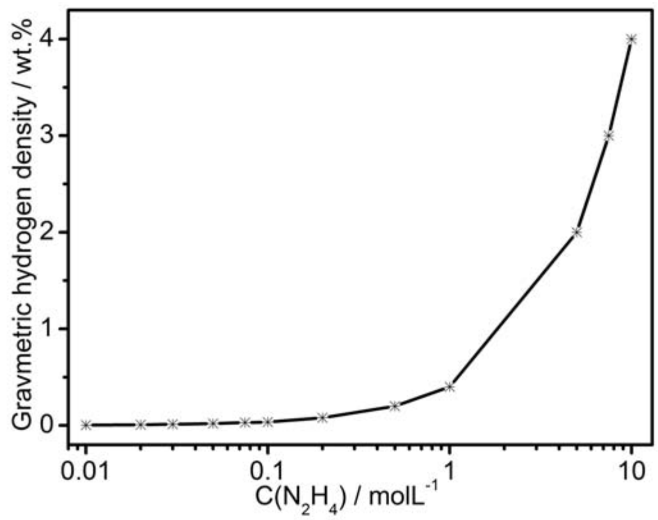

Fig.S17 Solution gravimetric hydrogen densities versus N_2H_4 concentrations for the decomposition of N_2H_4 over 4.6mg Co–B–N–H nanowires at 293K.

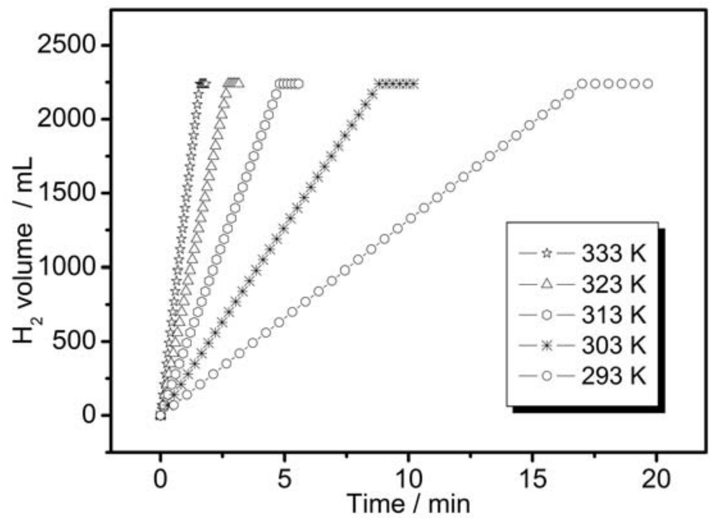

Fig.S18 Plots of volume of hydrogen generated versus time during the 20 mL N_2H_4 decomposition over 4.6mg Co–B–N–H nanowires at different temperatures in the range 293-333K ($[N_2H_4]$ = 5 $molL^{-1}$).

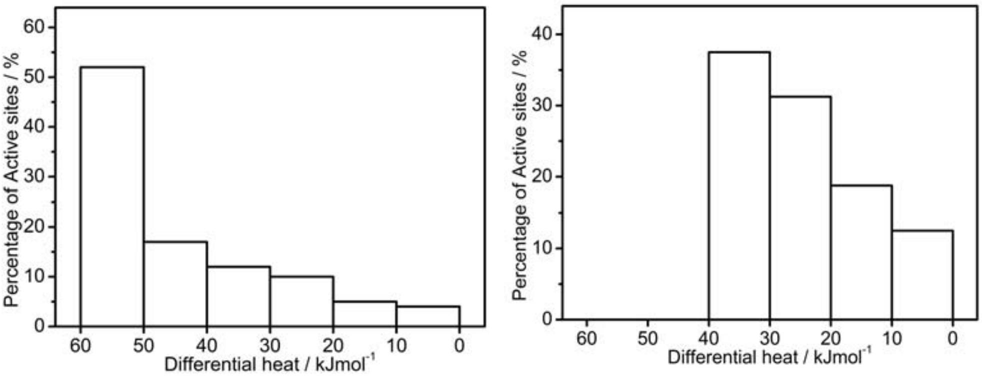

(a) (b)

Fig.S19 The differential heat of H_2 adsorption distribution histograms of (a) Co–B nanowires and (b) Co–B–N–H nanowires.

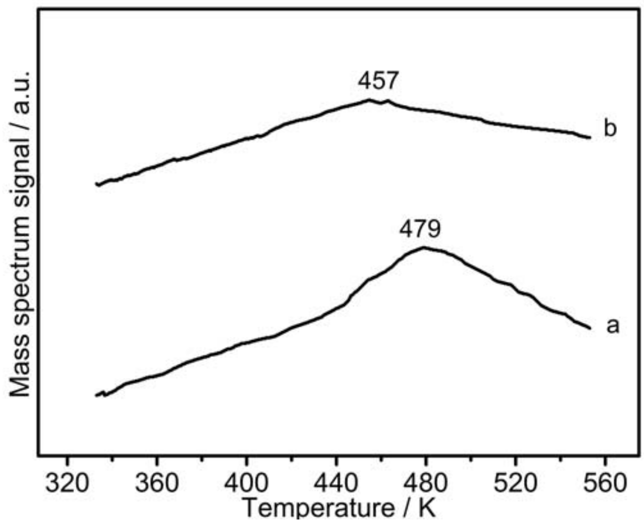

Fig.S20 Mass spectra of H_2-TPD for (a) Co–B nanowires and (b) Co–B–N–H nanowires.

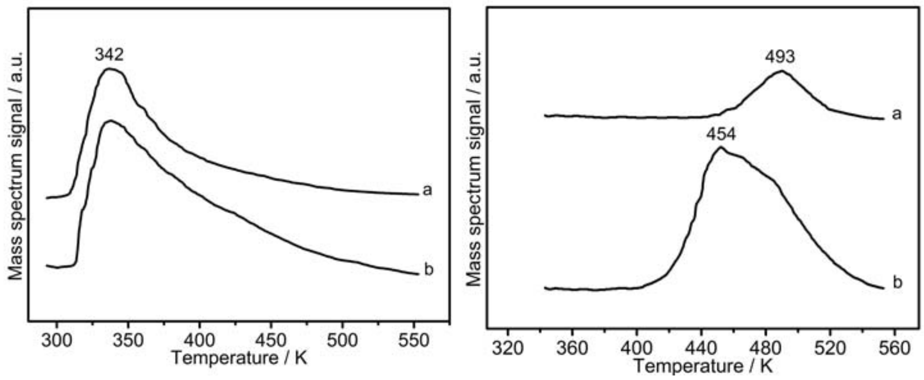

(A) (B)

Fig.S21 Mass spectra of NH_3 TPD-MS for (A) NH_3 desorption signal and (B) N_2 desorption signal for (a) Co–B nanowires and (b) Co–B–N–H nanowires.

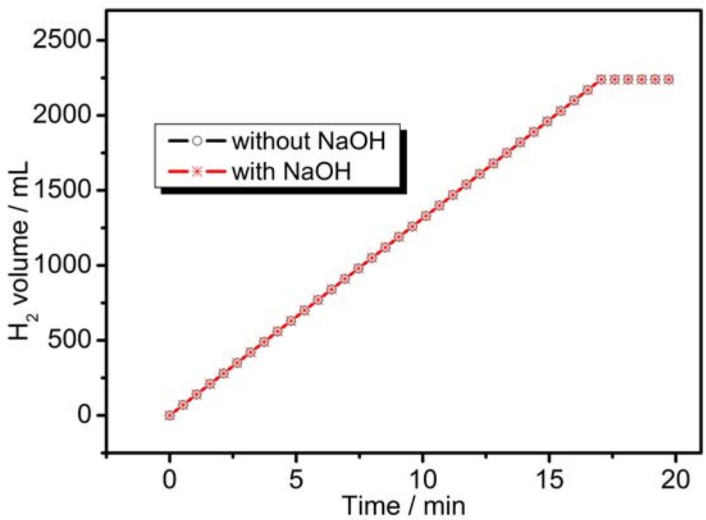

Fig.S22 Plots of volume of hydrogen generated versus time (a) without adding and (b) adding NaOH during the hydrazine decomposition over Co–B–N–H nanowires.

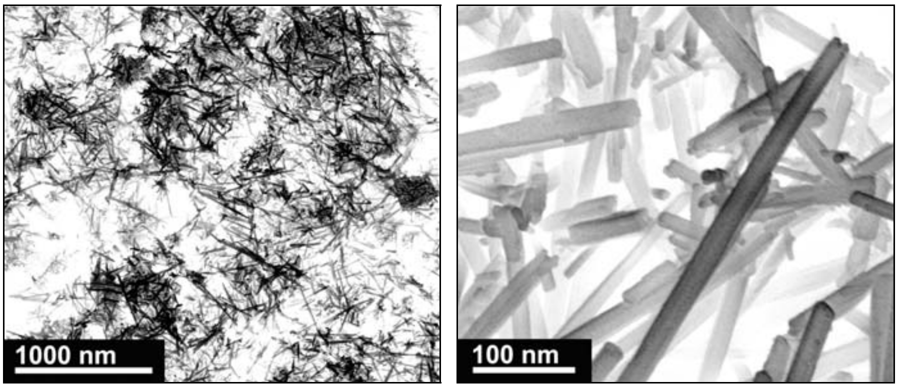

(a) (b)

Fig.S23 (a) STEM image and (b) enlarged STEM image of the deactivated Co–B–N–H nanowires.

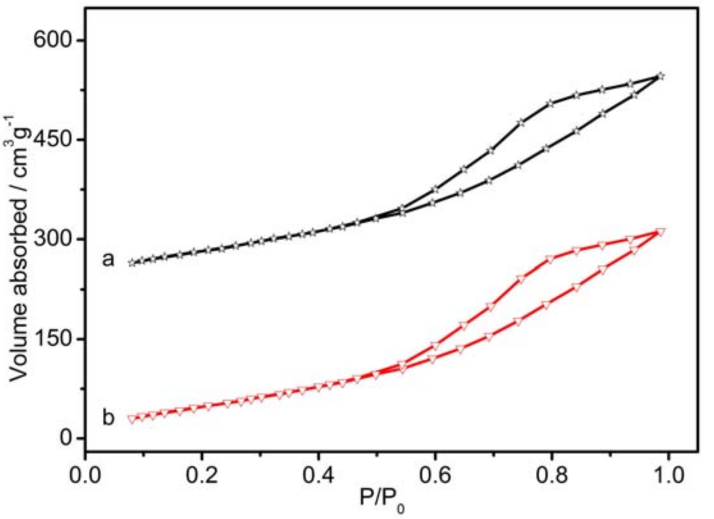

Fig.S24 Nitrogen sorption isotherms of the deactivated Co–B–N–H nanowires (a) before reactivation and (b) after reactivation by solution plasma process.

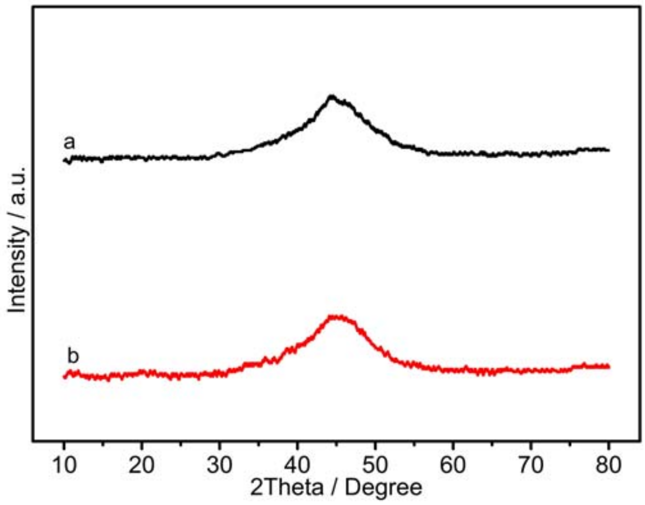

Fig.S25 XRD profiles of the deactivated Co–B–N–H nanowires (a) before reactivation and (b) after reactivation by solution plasma process.

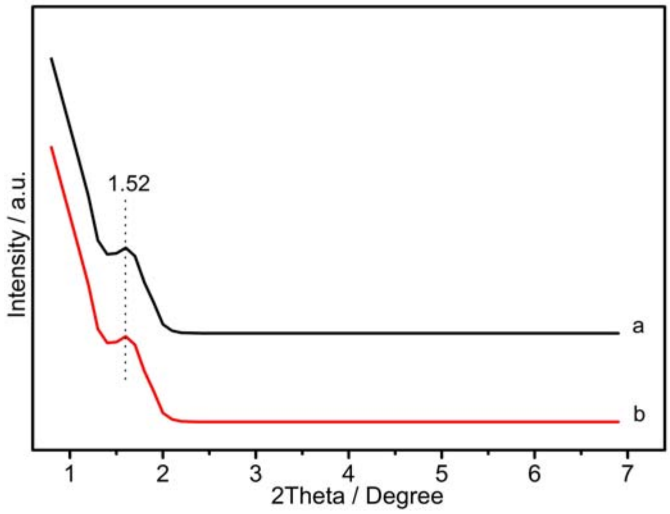

Fig.S26 Small angle XRD profiles of the deactivated Co–B–N–H nanowires (a) before reactivation and (b) after reactivation by solution plasma process.

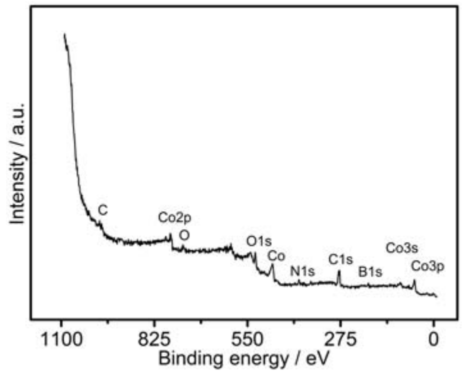

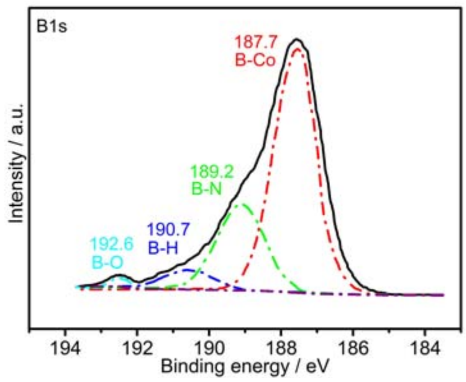

(a) (b)

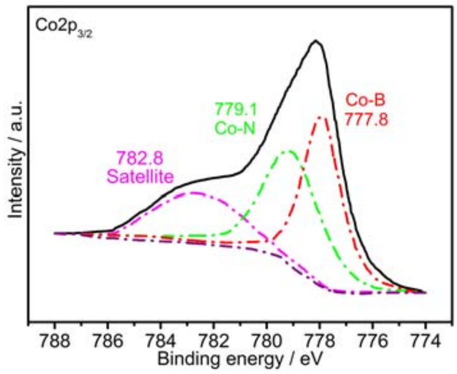

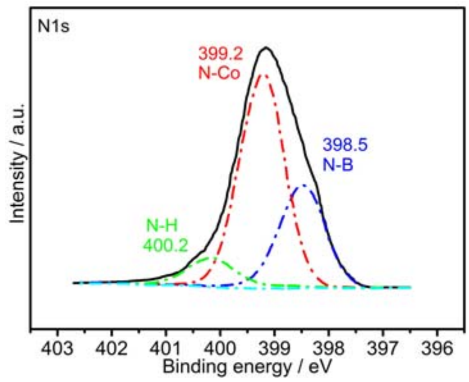

(c) (d)

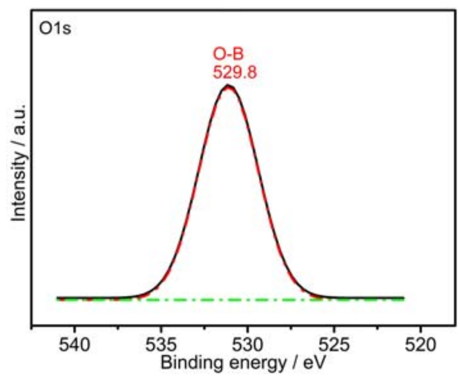

(e)

Fig.S27 (a) Overall XPS spectrum; (b) B1s XPS spectra; (c) Co2p3/2 XPS spectra and (d) N1s XPS spectra and (e) O1s XPS spectra of the deactivated Co–B–N–H nanowires.

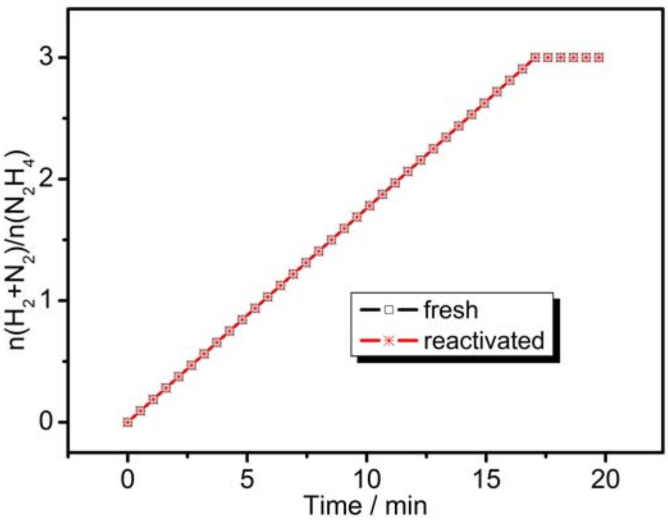

Fig.S28 Time profiles for decomposition of hydrous hydrazine in the presence (a) fresh and (b) reactivated Co–B–N–H nanowires.

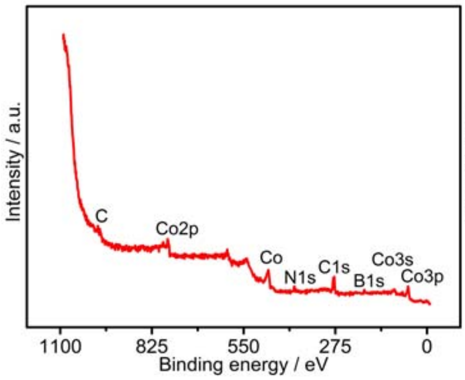

(a)

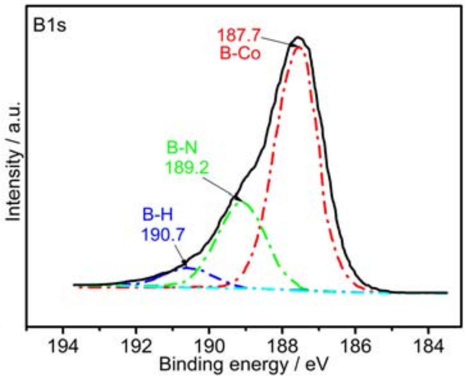

(b)

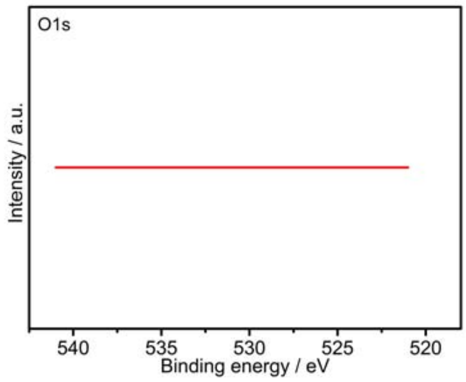

(c)

Fig.S29 (a) Overall XPS spectrum; (b) B1s XPS spectra and (c) O1s XPS spectra of the deactivated Co–B–N–H nanowires after reactivation by solution plasma process.

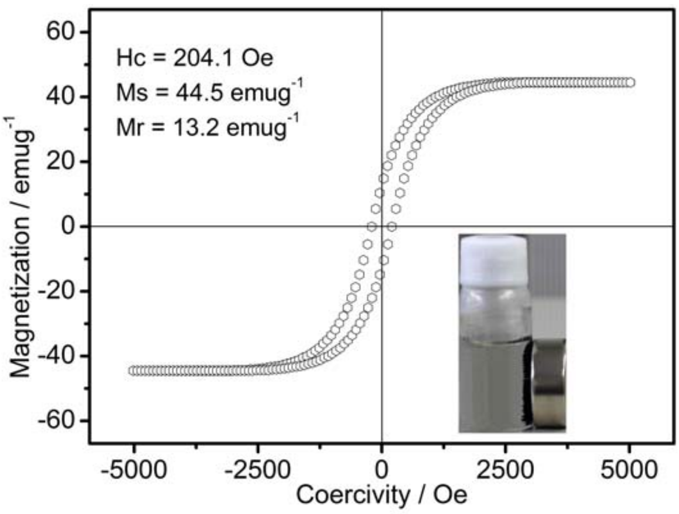

Fig.S30 Hysteresis loop and magnetic properties of Co–B–N–H nanowires. The inset is the photograph of Co–B–N–H nanowires after magnetic separation.

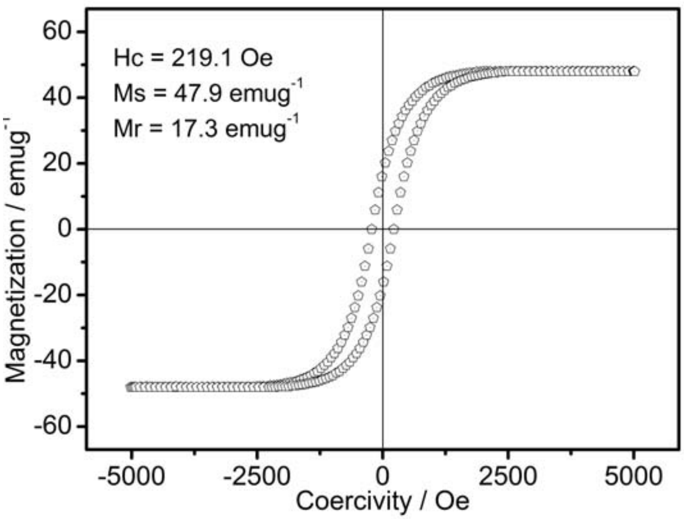

Fig.S31 Hysteresis loop and magnetic properties of Co–B nanowires.